

# Network-based genetic monitoring of landscape fragmentation

Ohad Peled<sup>1</sup>, Jaehee Kim<sup>2</sup>, and Gili Greenbaum<sup>1</sup>

<sup>1</sup>*Department of Ecology, Evolution and Behavior, The Hebrew University of Jerusalem, Jerusalem, Israel*

<sup>2</sup>*Department of Computational Biology, Cornell University, Ithaca, NY, US*

**Corresponding author:** Gili Greenbaum ([gil.G@mail.huji.ac.il](mailto:gil.G@mail.huji.ac.il))

## Abstract

Habitat fragmentation is one of the most immediate and substantial threats to biodiversity, generating isolated populations with reduced genetic diversity. Genetic monitoring has become essential for detecting fragmentation and tracking its progress. However, the coherent interpretation of genetic monitoring data and understanding the genetic consequences of fragmentation require frameworks that accurately represent real-world complexity. Existing theoretical frameworks typically rely on simplified spatial structures and do not adequately capture the heterogeneous migration patterns of natural populations. Here, we integrate network theory and mathematical population genetics to develop a framework for studying the genetic consequences of fragmentation processes, explicitly accounting for heterogeneous connectivity and temporal dynamics. We apply this framework to examine how different fragmentation processes affect genetic measures commonly used in genetic monitoring. We find that different fragmentation scenarios produce substantially distinct trajectories in key genetic measures, sometimes exhibiting rapid transitional dynamics, suggesting that the interpretation of genetic monitoring data must be tailored to ecological contexts. Furthermore, fragmentation can cause deviations from classical theoretical expectations, such as the expected correlation between genetic and geographic distance (isolation-by-distance) or between genetic diversity and connectivity. Finally, we propose and demonstrate detectable early warning signals in genetic monitoring data that precede rapid transitional phases. Our framework thus provides a practical interpretation of genetic monitoring data, bridging the gap between idealized theoretical models and real-world connectivity dynamics.

# 1 Introduction

Rapid human-induced environmental changes affect ecological and evolutionary processes, driving biodiversity loss [1]. One of the main factors driving these changes is landscape fragmentation, the partitioning of landscapes into small and weakly connected habitat patches [2]. Fragmentation reduces connectivity among populations, constraining gene flow and dispersal of individuals [3], which can negatively impact the health and viability of populations [4–6]. Landscape fragmentation is expected to erode within-population genetic diversity and increase between-population genetic differentiation due to reduced gene flow and increased genetic drift [7, 8]. Decreased genetic diversity can, in turn, reduce population viability in the short term by increasing risks of inbreeding depression [7, 9], while also limiting long-term evolutionary potential and adaptive capacity in response to future environmental changes [10, 11]. Consequently, systematically and coherently tracking fragmentation dynamics and their population-genetic consequences through genetic monitoring remains a major goal in conservation biology.

Genetic monitoring of population genetic metrics over time is a cost-effective and direct approach for tracking both the genetic impacts and the underlying ecological processes of fragmentation. The alternative, tracking individual movement among habitat patches, is usually resource-intensive and offers only an indirect proxy for the genetic and evolutionary consequences of fragmentation. Consequently, genetic monitoring of wild populations is widely used to assess population health and viability, landscape connectivity, and species responses to environmental disturbances [12–14]. However, a major challenge in applying genetic monitoring to track fragmentation lies in the interpretation of genetic measures in the context of the ecological process of migration.

Early theoretical work in population genetics established foundational frameworks for linking genetic diversity and differentiation to migration under simplified assumptions about gene flow patterns and spatial configurations [15–17]. For example, the island model assumes equal and constant migration rates without explicit spatial arrangement [15], whereas the stepping-stone model incorporates homogeneous and symmetric migration between adjacent demes arranged on a regular lattice with an additional long-range migration component [17]. These models provided fundamental insights into how spatial connectivity shapes population genetic structure and introduced key concepts such as isolation-by-distance, where genetic differentiation increases with geographic distance [18], and the connectivity-diversity relationship, in which populations that are more connected are expected to exhibit higher genetic diversity [19]. However, their simplified assumptions often limit their practical applicability for genetic monitoring and evaluating fragmentation impacts [20]. For example, one critical limitation of most existing modeling frameworks is their inability to capture the temporal dynamics of fragmentation, where landscape degradation and connectivity loss occur as heterogeneous, sequential processes shaped by the specific spatial and temporal characteristics of anthropogenic or climatic drivers [21]. The lack of a modeling framework that integrates realistic spatiotemporal patterns of connectivity and fragmentation thus restricts the practical application of population genetic theory in conservation efforts and limits its utility for informing management

39 decisions.

40 A promising approach for incorporating realistic gene flow patterns into population genetic  
41 theory is to represent connectivity between populations as a network—a mathematical construct  
42 comprising nodes (habitat patches) connected by edges (connectivity) [22]. Population networks  
43 can accommodate complex connectivity patterns beyond the scope of classical population genetics  
44 models. Several methods have been developed to infer such networks from genetic data by quanti-  
45 fying genetic differentiation between population pairs [23–25], with applications across a wide range  
46 of taxa [23, 26–32]. These network-based approaches provide a rigorous framework for modeling  
47 realistic fragmentation dynamics, enabling more coherent interpretations of genetic monitoring.

48 In this work, to bridge the gap between theory and practice, we develop a framework based  
49 on population networks, integrating advances in population-genetic theory and network science to  
50 investigate the spatiotemporal genetic consequences of landscape fragmentation. This framework  
51 explicitly incorporates real-world complexities within a conceptually simple and tractable model.  
52 We apply this framework to examine how different fragmentation scenarios affect genetic measures  
53 and to assess how network structure impacts population resilience under connectivity loss. While  
54 fragmentation is a multifaceted process involving multiple concurrent stressors (e.g., habitat loss,  
55 reduced patch size, edge effects), our focus here is on connectivity loss (also termed fragmentation  
56 *per se*; [5, 33]). Our approach enables improved interpretation of genetic monitoring data and  
57 facilitates identification and measurement of fragmentation progression. Additionally, our modeling  
58 framework can assist in predicting the genetic impacts of connectivity loss and evaluating the genetic  
59 health of fragmented populations.

## 60 2 Results

61 To model the genetic consequences of fragmentation, we consider a metapopulation in which some  
62 populations are connected by migration. For tractability, we assume equal and symmetric migra-  
63 tion rates among all connected populations. Any such connectivity pattern can be represented as  
64 a population network (Fig. 1a). To relate migration patterns to genetic measures, we employ the  
65 approach developed by Alcala *et al.* [34], which consists of two transformations: (i) from migra-  
66 tion matrices to pairwise coalescent-time matrices [35], and (ii) from coalescent-time matrices to  
67 pairwise genetic differentiation measured by  $F_{ST}$  [36] (see *Methods* and Supplementary Information  
68 Text). This procedure provides, for a given migration matrix, expected pairwise  $F_{ST}$  between all  
69 population pairs, as well as genetic diversity measured by expected heterozygosity ( $H_e$ ) for each  
70 population (Fig. 1a). For simplicity, we further assume uniform population sizes and mutation  
71 rates across all populations, allowing us to use an ‘unscaled’ heterozygosity measure (see *Methods*);  
72 therefore, our  $H_e$  values should be interpreted only relatively, and values exceeding one are possible.

73 To simulate an ecologically plausible metapopulation, which is usually embedded in a geographic  
74 landscape, we use a random geometric graph (RGG) model [37] as the initial network. In this model,  
75 populations are more likely to be connected if they are geographically close to each other. We model

76 a fragmentation process by iteratively removing edges according to one of several predefined frag-  
 77 mentation scenarios (Fig. 1b). After each edge removal, we recompute genetic measures, tracking  
 78 their changes until all edges have been removed and the network has become fully fragmented into  
 79 isolated populations. This modeling framework is highly flexible and enables the study of diverse  
 80 connectivity patterns and fragmentation scenarios while providing rigorous analytical expectations  
 81 for key genetic measures commonly used in genetic monitoring.

82 We consider eight fragmentation scenarios (Fig. 1b): (i) random fragmentation, representing  
 83 global environmental changes (e.g., climate change); (ii) autocorrelated fragmentation, representing  
 84 spatially correlated landscape disturbances (e.g., agricultural expansion); (iii) intrusive fragmenta-  
 85 tion, representing the emergence of isolated habitats within the landscape; (iv) regressive fragmen-

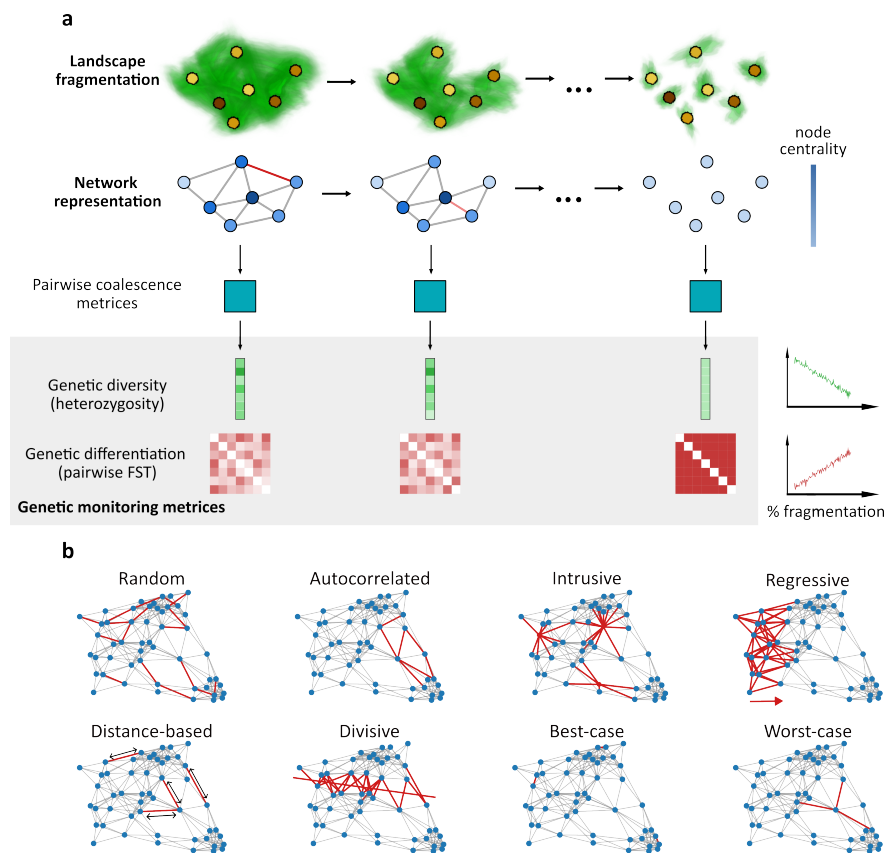


Figure 1: **Schematic representation of the network-based framework for modeling population genetic effects of fragmentation.** (a) Computation of genetic measures along fragmentation. In the top row, populations (yellow/brown patches) are embedded in a landscape (green) undergoing fragmentation. Below, the metapopulation is represented as a network with nodes (blue) denoting populations and edges representing migration between populations. Fragmentation is simulated by iteratively removing edges (red). A coalescence matrix is derived from each network, which enables the calculation of genetic diversity and differentiation at each fragmentation step (grey box). These metrics allow monitoring of population genetic changes over time (right side of the grey box). Color intensity of nodes represents network properties associated with genetic measures. (b) Modeling fragmentation processes. Illustrated are eight fragmentation scenarios applied to a single realization of a random geometric graph (RGG). Edges removed under each scenario are shown in red. Further details of each scenario are provided in the text.

86 tation, representing the expansion of a disturbance into a natural landscape (e.g., urban expansion);  
 87 (v) distance-based fragmentation, representing reduced dispersal ability through a non-habitable  
 88 matrix (e.g., disturbances hindering dispersal through the matrix, reducing dispersal distances);  
 89 (vi) divisive fragmentation, representing linear destruction of connectivity (e.g., road or railway  
 90 construction); (vii) best-case fragmentation, an idealized scenario that sequentially removes the  
 91 least important edges, thus maximizing connectivity at each step; and (viii) worst-case fragmen-  
 92 tation, similar to the best-case scenario, except the most important edge is removed at each step.  
 93 The last two scenarios are theoretical constructs intended to establish upper and lower bounds for  
 94 genetic measures rather than to depict realistic fragmentation processes. Detailed descriptions of  
 95 each fragmentation scenario are provided in *Methods*.

## 96 2.1 Genetic monitoring measures strongly depend on the fragmentation sce- 97 nario

98 Across all fragmentation scenarios, we observe an increase in genetic differentiation and a decrease  
 99 in genetic diversity as fragmentation progresses (Fig. 2). However, the rate and pattern of these  
 100 changes vary substantially among scenarios. The slowest erosion of genetic diversity and the most  
 101 gradual increase in genetic differentiation were observed under the best-case scenario (pink curve  
 102 in Fig. 2), as expected. In contrast, the worst-case scenario exhibited the most rapid erosion of  
 103 genetic diversity and the steepest increase in differentiation (grey curve in Fig. 2). Thus, these  
 104 two theoretical extremes provide upper and lower bounds for the retention of genetic health in the  
 105 metapopulation, against which other fragmentation scenarios can be compared.

106 In the random and autocorrelated scenarios, the loss of diversity and increase in differentiation  
 107 are almost undetectable in the early stages of fragmentation but then become substantial at  $\sim 60\%$   
 108 fragmentation. This pattern is reflected in concave curves for genetic diversity and convex curves  
 109 for differentiation (blue and orange curves in Fig. 2). The distance-based scenario (purple curve in

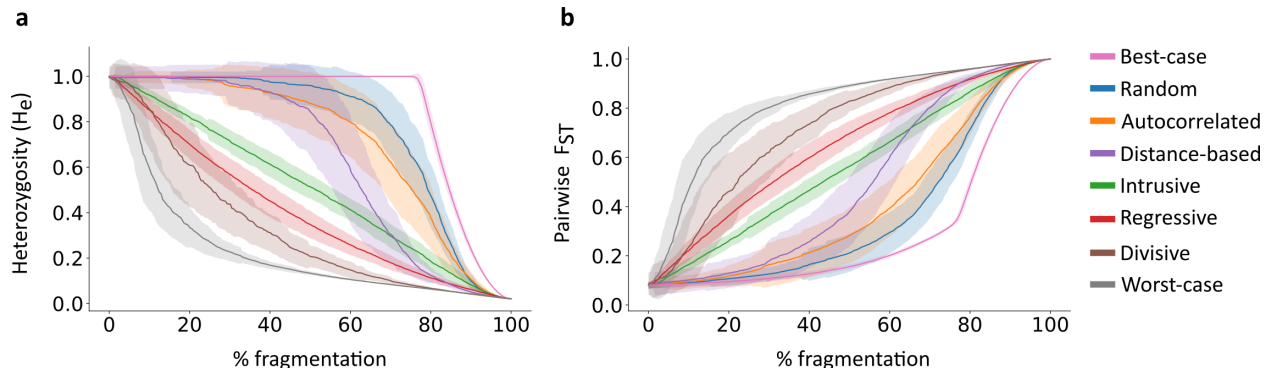


Figure 2: **Changes in genetic measures along fragmentation under eight fragmentation scenarios.** (a) Mean genetic diversity ( $H_e$ ) across all populations along fragmentation. (b) Mean genetic differentiation (pairwise  $F_{ST}$ ) among all population pairs. Lines denote means across 100 simulation replicates, with shaded regions indicating standard deviations. Fragmentation is measured as the fraction of edges removed from the initial network.

110 Fig. 2) shows a similar trend, but the loss of genetic diversity begins earlier in the fragmentation  
111 process and progresses faster than in the random and autocorrelated scenarios. In contrast, in the  
112 regressive and divisive scenarios, the curvature patterns are reversed: the genetic diversity curve is  
113 convex, with rapid and substantial decreases in genetic diversity early in the fragmentation process,  
114 and the genetic differentiation curve is concave, indicating earlier deterioration of metapopulation  
115 genetic health compared to the other scenarios. For example, in the divisive scenario, a  $> 50\%$   
116 change in genetic measures occurs already by 25% of the fragmentation process (brown curve  
117 in Fig. 2). In the intrusive scenario, both genetic measures change approximately linearly as  
118 fragmentation progresses (green curve in Fig. 2).

119 To understand the robustness of these patterns, we also examined how  $F_{ST}$  and  $H_e$  measures  
120 change along fragmentation under different migration rates and initial network topologies (Figs. S1  
121 and S2). Overall, the patterns remain similar across different migration rates, except at low mi-  
122 gration rates, where the absolute values of  $F_{ST}$  are higher in the early stages of fragmentation  
123 (Fig. S1b). Similarly, the results remained consistent when the initial network topologies were  
124 generated using either the Erdős-Rényi model or a small-world network model instead of the RGG  
125 model (Fig. S2). However, the differences among fragmentation scenarios were less pronounced in  
126 these analyses, highlighting the importance of considering spatially explicit network models, such  
127 as the RGG model.

128 Overall, our results demonstrate that, for a given level of connectivity loss, the risk of inbreeding  
129 depression and the reductions in both evolutionary potential and between-population differentia-  
130 tion strongly depend on the type of fragmentation process experienced by the metapopulation.  
131 Therefore, the interpretation of genetic monitoring data must account for the context and drivers  
132 of fragmentation. For example, a 10% decrease in  $H_e$  might reflect gradual connectivity decline un-  
133 der intrusive fragmentation, whereas the same decrease under random fragmentation could indicate  
134 dramatic habitat deterioration.

## 135 **2.2 Relationship between heterozygosity and network components**

136 When considering the distributions of the genetic measures rather than just their means, we observe  
137 that  $H_e$  distributions remain largely unimodal throughout the fragmentation process, with a shift  
138 towards  $H_e = 0$  occurring as isolated nodes accumulate (Figs. 3a–c and S4a–e). Similarly, the  
139  $F_{ST}$  distributions exhibit increasing bimodality, with density accumulating at  $F_{ST} = 1$  as more  
140 nodes are separated into different components (Figs. 3d–f and S4f–j). Changes in the shape of  
141 these distributions along fragmentation are also reflected in the variance of genetic diversity across  
142 populations (Fig. 3g): the level of fragmentation that maximizes variance, as well as the maximum  
143 variance value, differs among fragmentation scenarios. The increase in  $H_e$  variance can make  
144 the detection of fragmentation—and genetic health in general—more challenging at intermediate  
145 fragmentation levels because more populations will need to be sampled to correctly characterize  
146 the genetic diversity state of the metapopulation.

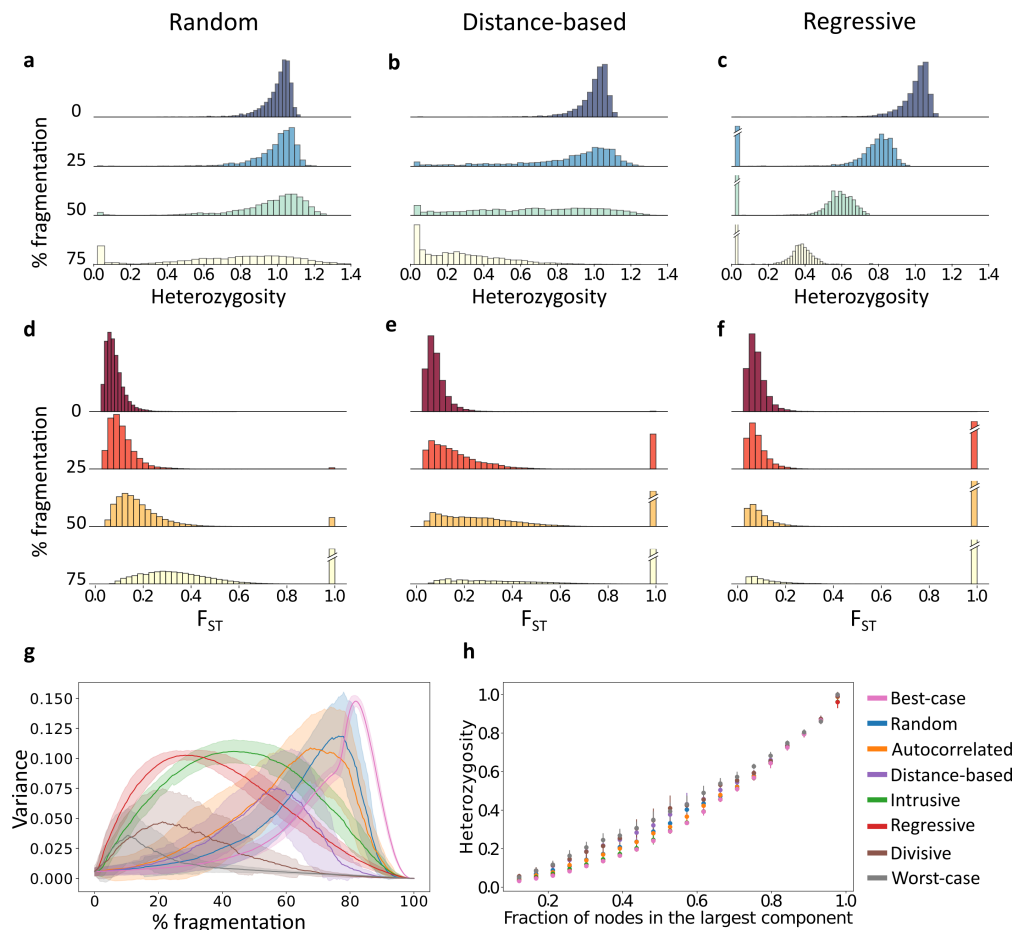


Figure 3: **Changes in the distributions of genetic measures along fragmentation.** Panels (a–f) show density distributions for three fragmentation scenarios: random, distance-based, and regressive (additional fragmentation scenarios are shown in Fig. S4). Four snapshots from the process are shown: 0%, 25%, 50%, and 75% fragmentation. Diagonal lines on bars indicate truncated values (for  $H_e = 0$  or  $F_{ST} = 1$ ). All distributions are pooled from 100 simulation replicates. (a–c) Distribution of expected heterozygosity ( $H_e$ ) of populations. (d–f) Distribution of pairwise  $F_{ST}$  across all population pairs. (g) Change in the variance of  $H_e$  across all populations in the network. (h) Relationship between the fraction of nodes in the largest component and mean  $H_e$  across all populations in each network. For each scenario, dots denote the means across 100 simulation replicates, and lines denote the standard deviations.

147 As fragmentation progresses, network structure changes and populations begin to disconnect  
 148 from the main component (Fig. S3). For example, the rapid deterioration in genetic health under  
 149 the divisive scenario (brown in Fig. 2) can be attributed to the early emergence of medium and  
 150 small network components, which reduce genetic diversity and increase between-component differ-  
 151 entiation (Fig. S3f). To better understand the effect of component structure on genetic diversity,  
 152 we tracked the size of the largest component throughout the fragmentation process (Fig. 3h). We  
 153 observe a strong correlation between the size of the largest component and the mean  $H_e$  across  
 154 populations in the network ( $r = 0.97$ – $0.98$  across scenarios,  $p$ -value  $< 0.001$ ). This correlation is  
 155 relatively consistent across different fragmentation scenarios, indicating that the size of the largest  
 156 component is an important determinant of genetic diversity.

157 This result can be interpreted in relation to the theoretical relationship between effective pop-  
158 ulation size and heterozygosity,  $H_e = \frac{4N\mu}{1+4N\mu}$  [38]. Because we consider a small effective population  
159 size relative to the mutation rate (i.e.,  $\theta = 4N\mu \ll 1$ ), we expect an approximately linear rela-  
160 tionship of  $H_e \approx 4N\mu$ . The result in Fig. 3h is similar to what one would expect if we treated  
161 each component as a well-mixed population. However, the relationship between  $H_e$  and component  
162 size is sublinear, reflecting the fact that components are not well-mixed and should therefore be  
163 represented with effective sizes smaller than their actual sizes.

### 164 2.3 Using network metrics in genetic monitoring

165 To better understand how tracking network characteristics can inform genetic monitoring, we eval-  
166 uated the association between genetic measures and commonly used network metrics. We first  
167 examined the relationship between a population’s genetic diversity and its centrality. There are  
168 different ways to measure network centrality [39], each of which can be interpreted differently with  
169 respect to population genetic processes [22]. Here, we evaluated two common metrics: degree  
170 centrality (i.e., the number of edges incident to a node), which measures local centrality, and be-  
171 tweenness centrality (i.e., the frequency with which a node lies on shortest paths between other  
172 nodes), which measures global centrality. Under classical population genetics theory, populations  
173 with higher connectivity should exhibit greater genetic diversity due to increased gene flow, leading  
174 to higher  $H_e$  at migration-drift equilibrium [19]. Consistent with this expectation, analysis of the  
175 initial (pre-fragmentation) networks showed a strong positive correlation between degree centrality  
176 and  $H_e$  ( $r = 0.71$ – $0.95$ , Fig. 4a). However, because all populations had a relatively high  $H_e$ , this  
177 relationship was nonlinear, exhibiting a saturating effect: while  $H_e$  increased with degree at low  
178 connectivity, it plateaued for highly connected nodes (Fig. S5a). Hence, local connectivity increases  
179 genetic diversity only up to a threshold, beyond which additional migration corridors do not sig-  
180 nificantly contribute to maintaining genetic diversity. In contrast, the association between  $H_e$  and  
181 betweenness centrality was weaker for nodes with low betweenness (Fig. S5b).

182 Throughout fragmentation, the correlation between  $H_e$  and degree centrality remains consis-  
183 tently high for some scenarios but declines rapidly early in the fragmentation process under the  
184 worst-case, divisive, and distance-based scenarios (Fig. 4a). This decline may result from network  
185 partitioning into components of varying size in these fragmentation scenarios, where component  
186 size has a stronger effect on  $H_e$  than does local connectivity. For example, a densely connected  
187 population in a small component with few populations may have lower  $H_e$  than a sparsely con-  
188 nected population in a larger component with many populations. Thus, component size, rather  
189 than degree centrality, is a primary determinant of genetic diversity at these intermediate frag-  
190 mentation stages. Interestingly, in these scenarios, the correlation later rebounds, converging to  
191 levels similar to those of the other fragmentation scenarios. This suggests that once components  
192 reach comparatively small sizes, within-component degree centrality once again becomes a strong  
193 determinant of  $H_e$ .

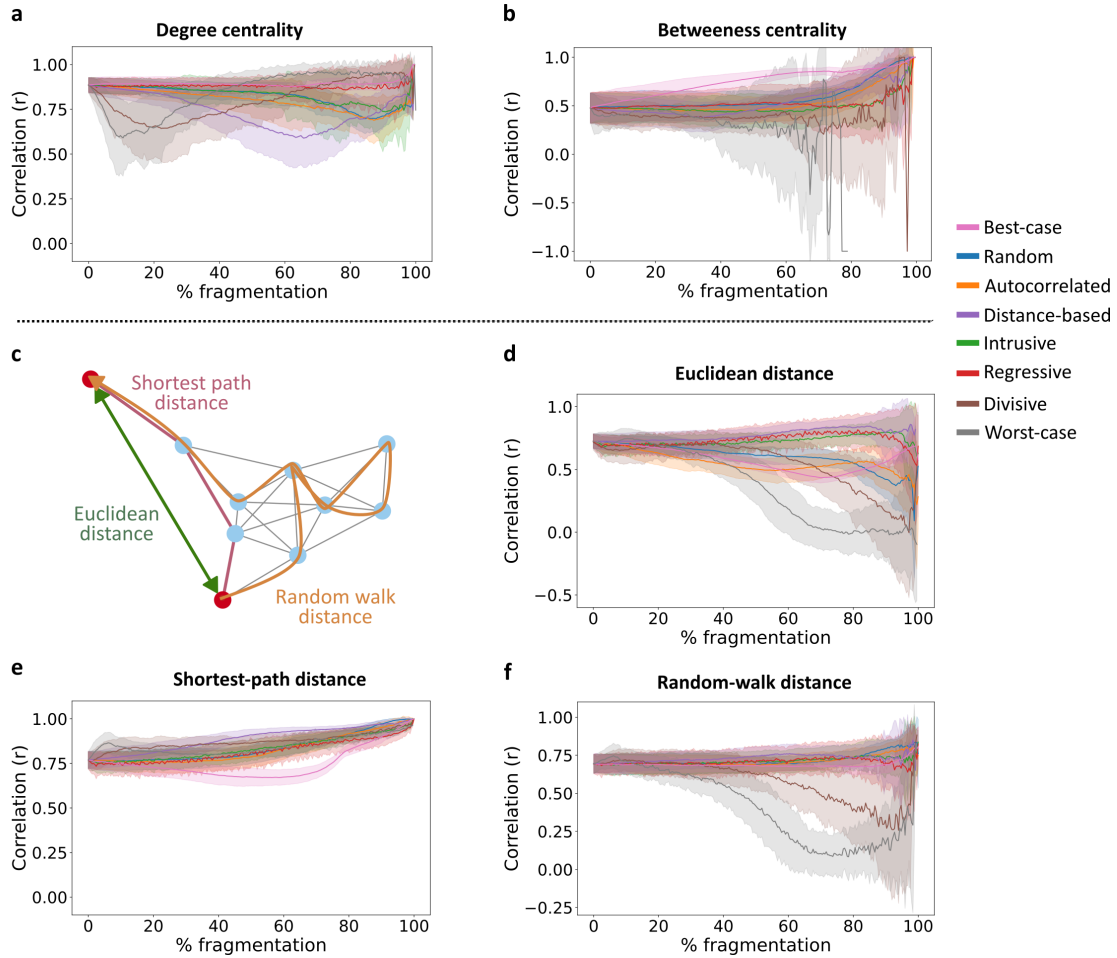


Figure 4: **Correlation between population genetic measures and network metrics.** The Pearson correlation coefficient  $r$  was computed between genetic diversity ( $H_e$ ) and network centrality (panels a–b), or between genetic differentiation ( $F_{ST}$ ) and distance metrics (panels c–f), for eight fragmentation scenarios. (a) Correlation between a population’s  $H_e$  and its degree centrality (number of connected edges). (b) Correlation between a population’s  $H_e$  and its betweenness centrality (global centrality metric). (c) Schematic illustration of three different distance metrics for a pair of populations (red nodes). (d) Correlation between the  $F_{ST}$  of a pair of populations and their Euclidean distance in the two-dimensional space in which the RGG network is embedded. (e) Correlation between the  $F_{ST}$  of a pair of populations and their shortest-path network distance. (f) Correlation between the  $F_{ST}$  of a pair of populations and their random-walk network distance.

194 The association between genetic diversity and betweenness centrality was generally weaker than  
 195 that for degree centrality, with less variation among fragmentation scenarios (Fig. 4b). This suggests  
 196 that populations do not necessarily need to occupy a key gene flow hub to maintain high genetic  
 197 diversity, as has been observed in some systems [40]. One implication of this is that peripheral  
 198 populations in large, well-connected networks can maintain genetic diversity comparable to that of  
 199 central populations in smaller, less connected components.

200 Next, we examined the relationship between pairwise  $F_{ST}$  and three network distance met-  
 201 rics relevant for genetic monitoring (Fig. 4c): (i) Euclidean distance in the two-dimensional space

202 of the embedded RGG network, (ii) shortest-path distance (the minimum number of edges re-  
203 quired to connect a pair of nodes), and (iii) random-walk distance (the expected number of edges  
204 traversed in a random walk between two nodes). Euclidean distance represents the geographic  
205 distance, whereas estimating the network distances requires knowledge of migration or movement  
206 patterns in the metapopulation [22]. Prior to fragmentation, we observed strong correlations be-  
207 tween  $F_{ST}$  and all three distance metrics ( $r = 0.7\text{--}0.75$ , Fig. 4d–f), indicating that geographically  
208 distant populations are more genetically differentiated irrespective of how distance is measured.  
209 This finding aligns with the isolation-by-distance expectation derived from stepping-stone [17] and  
210 continuous-space [41] models, suggesting that such idealized models are a good approximation for  
211 sufficiently well-connected networks [22]. However, as fragmentation progresses, these correlations  
212 vary substantially both over the course of fragmentation and among scenarios (Fig. 4d–f).

213 For Euclidean distance, the correlation declines under most fragmentation scenarios, particularly  
214 under the worst-case, divisive, best-case, and autocorrelated scenarios (Fig. 4d). Interestingly,  
215 these processes differ substantially in their network structure during fragmentation, particularly  
216 in the size of the largest connected component (Fig. S3), indicating that additional topological  
217 properties are needed to account for the relationship between genetic differentiation and geographic  
218 distance. In contrast, for shortest-path distance, the correlation consistently increases across most  
219 processes we examined (the theoretical best-case scenario is the exception) and generally shows the  
220 strongest association between  $F_{ST}$  and distance (Fig. 4e). This suggests that this network metric is  
221 particularly suited for genetic monitoring, either as a non-genetic proxy for genetic differentiation or  
222 as a proxy for connectivity from pairwise  $F_{ST}$  data. For the random-walk distance, the relationship  
223 remains relatively stable throughout fragmentation for most scenarios, except for a decline in the  
224 worst-case and divisive scenarios (Fig. 4f).

225 Overall, these analyses highlight that the topological properties of population networks can  
226 inform the tracking of genetic diversity and differentiation patterns. However, relating genetic  
227 measures to network properties such as components, centrality, or distance measures should, in  
228 most cases, be done in the context of the fragmentation scenario. Classical population genetic  
229 relationships—such as those between gene flow and diversity or distance and differentiation—are  
230 useful for well-connected populations but may diverge from classical theory when fragmentation  
231 processes shape the topology of metapopulation connectivity.

## 232 **2.4 Early warning signals in genetic monitoring**

233 The goal of genetic monitoring is to track the genetic health of populations and to infer under-  
234 lying ecological processes. However, our findings suggest that inferring fragmentation solely from  
235 genetic metrics can be challenging because substantial shifts in genetic measures often occur only  
236 in the later stages of fragmentation under certain fragmentation scenarios. In such cases, once  
237 genetic diversity declines and population differentiation increases, the transition is both rapid and  
238 pronounced (Fig. 2). This transition can be considered a tipping-point phase, before which it is

239 difficult to detect ongoing fragmentation by tracking the means of  $H_e$  and  $F_{ST}$ . This raises the  
240 question: Can genetic monitoring data detect landscape fragmentation early enough—before the  
241 population transitions to a highly fragmented and diversity-depleted state? In other words, if we  
242 are tracking genetic measures in a metapopulation that is progressively undergoing fragmentation,  
243 can we use genetic data to provide an early warning signal prior to the tipping-point phase during  
244 which genetic diversity and differentiation dramatically change? To address this question, we eval-  
245 uated whether early warning signals can be extracted from genetic diversity measures, borrowing  
246 methods from complex systems theory [42, 43]. Our analysis provides proof-of-concept for the  
247 potential to integrate early warning methodologies into genetic monitoring frameworks.

248 For this demonstrative analysis, we focused on the genetic diversity under the autocorrelated  
249 fragmentation scenario, where edges are removed in a spatially coordinated manner. We first con-  
250 sidered a genetic monitoring scheme that tracks the  $H_e$  distributions of all populations throughout  
251 fragmentation (Fig. 5a). At each time step, we analyzed the distribution of  $H_e$  across populations  
252 and computed several summary statistics—standard deviation, skewness, and kurtosis—which have  
253 been found to be reliable early warning indicators in other disciplines [44, 45]. Another common  
254 statistic, lag-1 autocorrelation, was not used because it is intended to measure stability around  
255 a single equilibrium [44, 46], which did not hold in our simulations. As the metapopulation ap-  
256 proaches the tipping-point phase, the theoretical expectation is that the standard deviation of the  
257  $H_e$  distribution will increase, the skewness will shift toward the new state (in this case, asymmetry  
258 towards lower  $H_e$  values), and the kurtosis will increase due to an increased frequency of extreme  
259 values [43, 45]. To evaluate this, we computed these summary statistics throughout fragmenta-  
260 tion (green curves in Fig. 5b–d) and examined whether they show substantial changes prior to the  
261 tipping-point phase (the sharp drop in the orange curves at  $\sim 80$ – $90\%$  fragmentation in Fig. 5b–d).

262 Some early warning signals prior to the tipping-point phase were clearly observable in our  
263 analyses (Fig. 5b–d). For example, the standard deviation of the distribution of  $H_e$  across the  
264 metapopulation increases steadily as fragmentation progresses, and substantial changes in this  
265 statistic are observable at the early stages of fragmentation even when changes in the mean are not  
266 yet detected (Fig. 5b). Thus, by tracking the standard deviation among populations over time, a  
267 noticeable change in this summary statistic could be identified and used as an early warning signal  
268 before the tipping-point phase. The mean skewness and kurtosis also showed early changes that  
269 can serve as early warning signals (Fig. 5c–d). However, the trajectories of skewness and kurtosis  
270 fluctuated over time and were noisier than the standard deviation, suggesting that they are less  
271 reliable as early warning indicators. This means that, while tracking the mean metapopulation  
272  $H_e$  would not indicate that a rapid reduction in genetic health is approaching, monitoring higher  
273 moments could potentially provide an early indication of genetic deterioration.

274 We also considered a more limited monitoring scenario, where  $H_e$  is monitored for a single  
275 population (Fig. 5e). In this setting, a single population is tracked over time, and we evaluate the  
276  $H_e$  distribution of 25% sliding temporal windows throughout fragmentation. As with the previous  
277 scenario, we tracked changes in the summary statistics of the distributions along fragmentation.

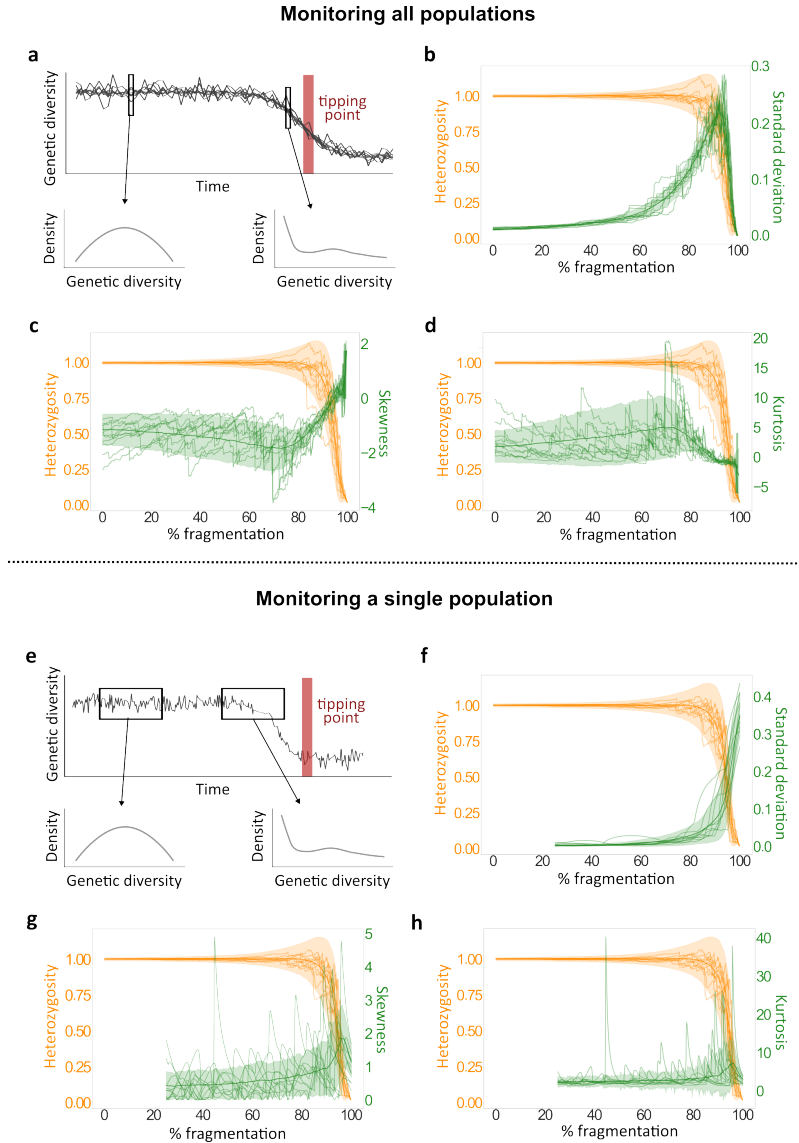


Figure 5: **Early warning signals before tipping point in genetic monitoring.** The analysis examines fragmentation under the autocorrelated scenario (Fig. 1b). (a) Schematic of the metapopulation-monitoring approach. At each time step, we analyze the  $H_e$  distribution of all connected populations in the network (largest component). The tipping-point phase, during which genetic diversity dramatically declines, is denoted in red. Genetic diversity distributions closer to the tipping-point phase may differ, with summary statistics potentially providing early warning. (b–d) Mean metapopulation heterozygosity (orange) and three early warning statistics (green: SD in (b), skewness in (c), and kurtosis in (d)) along fragmentation. Solid lines show the mean across 1000 simulation replicates, shaded areas show the standard deviation, and thin lines show ten individual replicates. (e) Schematic of the single-population monitoring approach. The  $H_e$  of a single population is tracked with a sliding window; the  $H_e$  distributions in each window are then analyzed. The tipping-point phase is shown in red. As above, the genetic diversity distributions in windows closer to the tipping-point phase may differ, with summary statistics potentially providing an early warning. (f–h) Mean metapopulation heterozygosity (orange) and three early warning statistics computed from 25% of the data per window (green: SD in (f), skewness in (g), and kurtosis in (h)). Solid lines show the mean across 1000 simulation replicates, shaded areas show the standard deviation, and thin lines show ten individual replicates.

278 Unlike the scenario that tracks the entire metapopulation, here we were not able to identify substan-  
279 tial early warning signals (Fig. 5f–h). While the standard deviation did increase as fragmentation  
280 progressed, the change was not substantial prior to the tipping-point phase (Fig. 5f). Although  
281 no directional change in kurtosis was observed, skewness showed a moderate early increase, which  
282 could potentially provide some early warning (Fig. 5g, h). Taken together, our analyses indicate  
283 that under the simulation settings examined, cross-sectional monitoring of multiple populations  
284 at each sampling occasion yields earlier and more reliable early warning signals than tracking a  
285 single population through time, even when the latter is summarized over an extended temporal  
286 window. The likely reason is that the cross-sectional snapshot includes multiple quasi-independent  
287 observations per time step, whereas the sliding-window yields serially autocorrelated records.

### 288 3 Discussion

289 Habitat fragmentation is one of the most pressing threats to global biodiversity [2, 47], and genetic  
290 monitoring could be instrumental in tracking and managing it. However, developing monitoring  
291 and intervention strategies that take into account the real-world complexities of population struc-  
292 ture remains a challenge [48, 49]. We present a framework that enables the modeling of habitat  
293 fragmentation and its impacts on population genetic measures, thereby expanding the potential  
294 scope of genetic monitoring. Using this framework, we model complex connectivity patterns and  
295 simulate temporal dynamics and spatially heterogeneous fragmentation processes. We examined  
296 the effects of different fragmentation scenarios on genetic measures and found that the same rate of  
297 fragmentation can lead to markedly different patterns of genetic differentiation between populations  
298 ( $F_{ST}$ ) and levels of genetic diversity within populations ( $H_e$ ). In this network-based perspective  
299 of fragmentation, we also find that classical population genetic relationships, such as the asso-  
300 ciation between  $F_{ST}$  and geographical distance or between gene flow and local genetic diversity,  
301 may not always hold. Network topology metrics can help interpret these associations. Finally, we  
302 demonstrate how genetic monitoring can potentially be used to detect early warning signals before  
303 fragmentation triggers critical shifts in the genetic health of populations.

304 The population network framework presented here can be applied to study many ecological  
305 processes that affect connectivity. Nonetheless, it is especially relevant in the context of genetic  
306 monitoring because it can inform how genetic measures in populations change over time [50].  
307 Human activity can induce fragmentation in different ways, but theoretical investigations of frag-  
308 mentation dynamics and their potential consequences have thus far been limited [21, 51]. Our  
309 results underscore the importance of considering the sequence of events leading to fragmentation  
310 for accurate evaluation of its progression. While we observe steady rates of genetic changes that  
311 are consistent with theory in some cases [52, 53], we also find scenarios in which genetic measures  
312 change abruptly (Fig. 2).

313 An important factor in shaping the temporal change in genetic measures is the maximum num-  
314 ber of connected populations in the network (i.e., the size of the largest component; Fig. 3h).

315 For example, scenarios in which a large component is maintained for a longer period (best-case,  
316 random, autocorrelated; Fig. S3) maintain the genetic health of populations longer (Fig. 2). This  
317 pattern holds even when populations within components are weakly or indirectly connected. From  
318 a landscape management perspective, it implies that enhancing connectivity between network mod-  
319 ules (i.e., clusters of connected populations) may be more beneficial for maintaining high levels of  
320 genetic diversity than increasing direct connectivity within a weakly connected module. This result  
321 is consistent with the expectation that larger populations (or metapopulations) will exhibit higher  
322 genetic diversity due to increased gene flow and decreased genetic drift at the global scale [38].  
323 However, increasing global connectivity can lead to homogenization of genetic pools and loss of  
324 local adaptations [54, 55]. Therefore, considering the spatial scale at which connectivity between  
325 populations is measured is crucial for accurately interpreting genetic monitoring outputs.

326 Populations and ecological systems facing environmental changes can undergo dramatic, unex-  
327 pected, and often irreversible transitions. In the context of tracking biodiversity, several studies  
328 have introduced the concept of fragmentation thresholds that lead to regime shifts in biodiversity  
329 [56–58]. However, regime shifts in terms of genetic health and population-level metrics have re-  
330 ceived far less attention and have been considered primarily in the context of adaptive evolution in  
331 response to stress [59]. Consequently, genetic monitoring of populations is often reduced to qualita-  
332 tive assessments. We demonstrated that genetic indicators may appear constant during substantial  
333 periods of fragmentation, followed by rapid shifts in genetic metrics (e.g., random or autocorrelated  
334 fragmentation in Fig. 2). This suggests that a standard interpretation of genetic monitoring—no  
335 genetic change over time implies no underlying fragmentation process—can be misleading. As a  
336 proof-of-concept, we showed that early warning signals may be detectable by tracking features of  
337 the distributions of genetic monitoring data. This is particularly true if a large number of popula-  
338 tions in the metapopulation are monitored. Although there is a substantial body of theoretical and  
339 statistical literature on early warning signals [42, 43, 46, 60], to the best of our knowledge, no theo-  
340 retical or empirical studies have explored the integration of these methods with population-genetic  
341 data so far. Further investigation, applying a more comprehensive suite of early warning methods  
342 (e.g., Kendall’s  $\tau$  statistic, conditional heteroskedasticity) to empirical data, may shed additional  
343 light on the effectiveness of this approach.

344 Patterns of spatial genetic structure have been extensively studied for almost a century, both  
345 in theoretical population genetic models [17, 18, 35, 61] and in empirical studies of natural pop-  
346 ulations [62–64]. One prevailing view is that spatial separation generates isolation-by-distance  
347 patterns reflected in genetic differentiation measures [17, 18, 65]. However, we find that these pat-  
348 terns may deviate from classical expectations depending on the underlying fragmentation scenario  
349 and the distance metric used (Fig. 4c–f). Similarly, the relationship between genetic diversity and  
350 connectivity [66–68], a key guideline in conservation practices [69], can also weaken during fragmen-  
351 tation (Fig. 4a–b). These findings highlight the need to integrate complex spatial configurations of  
352 populations and realistic descriptions of ecological processes into population genetic studies.

353 Although our framework is flexible and allows detailed spatial configurations, we assumed con-

stant population sizes and symmetric continuous migration rates, and we did not incorporate extinction-colonization dynamics. While our sensitivity analyses suggest that the way different fragmentation scenarios affect genetic measures is relatively general and not strongly affected by the initial network structure or migration rates, other ecological features may have important impacts. Our main goal, therefore, is to provide qualitative understanding of how genetic monitoring data should be interpreted, rather than to offer precise ways to represent realistic population dynamics. One important assumption in our model relates to the time required for a system to reach migration-drift equilibrium between fragmentation steps. When the rate of fragmentation is substantially faster than the rate of approach to equilibrium, our framework may not be appropriate. It has been suggested that genetic differentiation may respond more rapidly than heterozygosity to changes in migration [52] and reach equilibrium faster [70, 71]; therefore, in some cases, the framework may be suitable for tracking genetic differentiation but not genetic diversity.

As non-invasive population-genomic data become increasingly accessible, genetic monitoring is expected to emerge as a leading tool in conservation biology for assessing the health, ecology, and behavior of natural animal and plant populations. However, the gap between theoretical expectations and practical challenges in conservation biology currently limits our ability to accurately interpret genetic data and develop landscape-specific and species-specific conservation strategies. Our framework incorporates the real-world complexities of space and time and is readily interpretable in terms of genetic monitoring. Here, we explored an important aspect of fragmentation—the processes and patterns by which between-population connectivity is lost—but our framework can be readily expanded to investigate other anthropogenic effects, such as habitat loss (e.g., by simulating different node-removal processes) or the utility of interventions (e.g., prioritization of ecological corridors). Our network-based framework thus serves to narrow the gap between theoretical insights and the complex ecological realities of conservation biology.

## 4 Methods

All analyses were performed using Python 3.11.1, except where stated otherwise.

### 4.1 Computing genetic measures in population networks

To compute genetic measures for population networks, we employed the framework developed by Alcalá *et al.* [34], which integrates the mathematical relationship between migration and coalescence times by Wilkinson-Herbots [35] with the relationship between coalescent times and  $F_{ST}$  by Slatkin [36]. Our method relies on transformations among three matrices: (i) the migration matrix describing the pairwise migration rates, (ii) the coalescence matrix describing the expected time to coalesce for two lineages within or between populations, and (iii) the  $F_{ST}$  matrix describing the pairwise genetic distance between populations. A full explanation of the derivations and computations is presented in the Supplementary Information Text.

We considered an idealized system of  $K$  populations of equal size, evolving under the neutral

390 Wright-Fisher model at migration-drift equilibrium [19]. Let  $m_{ij}$  denote the backward migration  
391 rate from population  $i$  to  $j$ , representing the probability that a lineage in  $i$  originated in  $j$  in the  
392 previous generation. We assumed symmetric migration ( $m_{ij} = m_{ji}$  for all  $i$  and  $j$ ) to ensure con-  
393 servative migration [35], where total incoming and outgoing migration balance in each population:  
394  $\sum_{j \neq i} M_{ij} = \sum_{j \neq i} M_{ji}$ . While conservative migration is a weaker assumption than symmetric mi-  
395 gration, we imposed symmetric migration for tractability. Under these assumptions, the migration  
396 structure of the populations is represented as a symmetric, undirected network  $M$  of  $K$  nodes  
397 with zero-diagonal entries. For a pair of nodes  $i$  and  $j$  ( $i \neq j$ ), the weight assigned to the edge is  
398  $M_{ij} = 4Nm_{ij}$ , representing the expected number of migrants from  $i$  to  $j$  per generation, with  $N$   
399 denoting the population size of each of the nodes. We simulated population networks with  $K = 50$   
400 nodes, where migration rates are uniform across all edges ( $M_{ij} = 1$  in the main text, and alternative  
401 migration rates in Fig. S1).

## 402 4.2 Simulating fragmentation processes in population networks

403 Because natural populations are embedded in a geographic space, we used spatial network models  
404 [72], in which nodes correspond to populations with assigned geographic coordinates. We primarily  
405 used the random geometric graph (RGG) model [37], one of the simplest and most widely studied  
406 spatial network models, to generate the initial network in our simulations (see Fig. S2 for alternative  
407 network models). In this model,  $K$  populations are placed uniformly at random in a unit square in  
408 Euclidean space, and an edge is formed between two nodes if their Euclidean distance is below a  
409 fixed threshold  $d$ . The RGG model is particularly well-suited for representing migration in spatially  
410 structured populations because it captures the ecologically realistic constraint that migration occurs  
411 only between sufficiently proximate populations. The connectivity threshold for two-dimensional  
412 RGG networks (i.e., the value of  $d$  above which the network is almost surely connected) is  $\sqrt{\frac{\log K}{\pi K}}$   
413 [73], which equals  $d = 0.16$  for  $K = 50$ . We therefore set  $d = 0.30$ , which consistently generates a  
414 connected network that is not too dense yet sufficiently above the threshold at which the network  
415 is close to being disconnected.

416 To model the fragmentation process, we sequentially remove edges from the initial network, one  
417 at a time, until no edges remain. We consider eight fragmentation scenarios (Fig. 1). (i) *Random*  
418 *fragmentation*. At each fragmentation step, an edge is removed uniformly at random, representing  
419 non-specific habitat deterioration, such as fragmentation induced by global climate change. (ii)  
420 *Autocorrelated fragmentation*. Initially, one random edge is removed. At each subsequent step, one  
421 edge is removed uniformly at random from the set of edges adjacent to the previously removed edge  
422 (i.e., edges sharing a node with the last removed edge). This process models spatially correlated  
423 landscape disturbances, such as urban or agricultural expansions. (iii) *Intrusive fragmentation*.  
424 A node is selected uniformly at random, and all its incident edges are removed in random order.  
425 Once these edges are removed, another node is chosen randomly, its incident edges are removed, and  
426 the process is repeated. This process generates isolated habitable “islands” within the landscape,  
427 representing, for example, the formation of micro-reserves—small, disconnected populations. (iv)

428 *Regressive fragmentation.* Edges are sorted by the minimum x-coordinate of their incident nodes in  
429 the Euclidean plane and removed progressively from low to high x-coordinate values, starting with  
430 the edge having the smallest x-coordinate. This process represents large-scale spatial disturbances  
431 moving across the habitat, such as shifts in climate-change fronts. (v) *Distance-based fragmentation.*  
432 At each step, the edge connecting the most distant populations in the underlying Euclidean space is  
433 removed. This process represents a general environmental deterioration that impedes long-distance  
434 dispersal among habitat patches. (vi) *Divisive fragmentation.* A line is drawn in the Euclidean plane  
435 by connecting two points on different boundaries (either opposing or neighboring boundaries) of the  
436 metric space (selected uniformly at random), effectively bisecting the habitat. All edges intersecting  
437 this line are sequentially removed, starting with those having the smallest x-coordinate (as defined  
438 in (iv)). This process models the introduction of linear barriers, such as roads or railways, into  
439 the landscape. (vii) *Best-case fragmentation.* At each step, the edge with the lowest betweenness  
440 centrality is removed. Betweenness centrality was computed with the NetworkX Python library.  
441 Because such edges contribute minimally to network connectivity, removing them is expected to  
442 have the least impact on genetic measures. Although this scenario is not realistic, it serves as an  
443 upper benchmark for evaluating genetic measures at a given level of fragmentation. (viii) *Worst-*  
444 *case fragmentation.* Similar to best-case fragmentation, but at each step, the edge with the highest  
445 betweenness centrality is removed. This process provides a lower benchmark for genetic measures  
446 at a given level of fragmentation.

447 These eight fragmentation processes do not exhaustively cover all possible scenarios, but rather  
448 describe typical ecological and anthropogenic disturbance patterns relevant to genetic monitoring  
449 [21, 74]. Because these processes are stochastic, we performed 100 independent replicates per  
450 fragmentation type, randomizing the initial network configuration and the fragmentation sequence  
451 in each replicate.

452 In each simulation replicate, we computed the changes in  $F_{ST}$  and  $H_e$  distributions in response  
453 to fragmentation, assuming migration-drift equilibrium is reached between successive iterations  
454 of edge removal. Each replicate generates a sequence of migration matrices  $M_0, \dots, M_x$ , with  $x$   
455 being the last fragmentation step. From these migration matrices, we computed corresponding  
456  $F_{ST}$  matrices  $F_0, \dots, F_x$  and  $H_e$  vectors  $H_0, \dots, H_x$ . These sequences reflect the changes in genetic  
457 differentiation and genetic diversity throughout fragmentation. Using these sequences, we tracked  
458 changes in the means (Fig. 2), sample variances (Fig. 3g) and distributions (Fig. 3a–f) of the genetic  
459 measures along fragmentation.

460 We also evaluated changes in network structure throughout fragmentation by tracking for four  
461 structural categories: (i) largest component, (ii) other components with  $> 3$  populations (medium  
462 components), (iii) components of 2–3 populations (pairs/triads), and (iv) isolated nodes. At each  
463 time step, we computed the mean proportion of nodes in each category across simulation replicates.

464 To account for alternative patterns of gene flow in our initial network, and to evaluate their  
465 effect on our main conclusions, we considered two additional models. (i) The Erdős–Rényi (ER)

466 random network [75], in which, for  $K$  populations, each pair of populations is connected by an  
467 edge with probability  $p$ . To generate a well- but not fully-connected initial network, we set  $p = 0.1$   
468 (125 edges in total). To allow spatially explicit analysis that can be compared to the RGG, we  
469 embedded this model in Euclidean space, with nodes placed uniformly at random. (ii) The small-  
470 world Watts–Strogatz (WS) network is constructed by connecting each population (node) to its  $k$   
471 nearest neighbors in a ring topology, and then rewiring each edge with probability  $p$  to connect to a  
472 randomly chosen population (node), introducing long-range connections while preserving the total  
473 number of edges. The WS network can represent species with a life history of many short-distance  
474 dispersal events and an occasional long-distance dispersal event. We use a modified variant of this  
475 model to incorporate spatial characteristics to the network [76, 77]. We use the `grid_graph` function  
476 in the Python library NetworkX to generate a two-dimensional network with  $n$  nodes, setting  $k = 4$   
477 (4 neighbors for each node), and a re-wiring probability of  $p$ . This setting converges to the stepping  
478 stone model [17] for  $p = 0$ . For our simulations, we set  $n = 49$  (a  $7 \times 7$  matrix).

### 479 4.3 Correlations between genetic measures and node attributes

480 To investigate how network metrics influence genetic monitoring along fragmentation, we examined  
481 the relationship between genetic measures and network metrics. For each network at each frag-  
482 mentation step, we computed two node centrality measures, degree centrality (number of incident  
483 edges for the focal node) and betweenness centrality (how often a node lies on the shortest paths  
484 between other pairs of nodes), for all nodes in the network. We then computed the Pearson corre-  
485 lation coefficient ( $r$ ) between node’s  $H_e$  and their centrality score, at each fragmentation step and  
486 for each centrality measure (we excluded isolated nodes, for which centrality is undefined). Then,  
487 we computed the mean  $r$  and its  $SD$  for each fragmentation step across the simulation replicates,  
488 for each one of the centrality metrics and each fragmentation scenario. We only show significant  
489 correlation results ( $p < 0.05$ ) with data from 5 or more replicates.

490 Similarly, we evaluated the relationships between network distance metrics and pairwise  $F_{ST}$ .  
491 We computed the distance between all pairs of nodes in each fragmentation step using three distance  
492 metrics: (i) Euclidean distance, the standard geometric measure in the embedded metric space,  
493 analogous to the typical geographic distances among populations; (ii) shortest-path distance [78],  
494 calculated as the minimum number of edges needed to traverse from one node to another, reflecting  
495 topology-aware movement; (iii) random-walk distance [79], defined as the mean number of edges  
496 a random walker requires to travel from one node to another, which is suitable for movement  
497 that is unaware of the network topology or a non-targeted movement [22]. Random-walk distance  
498 was estimated using 50 random-walk iterations per pairwise comparison. The correlations were  
499 calculated only within connected components of size  $> 3$ , and pairs of nodes in disconnected  
500 components were excluded from correlation calculations (these pairs have  $F_{ST} = 1$  and are infinitely  
501 distant from each other for shortest-path and random walk distance). We computed the Pearson  
502 correlation coefficient ( $r$ ) between the  $F_{ST}$  of all node pairs and their distance score, at each  
503 fragmentation step and for each distance metric. We used the `mantel` python library to perform

504 a Mantel test and calculate a corresponding p-value with 999 permutations. For networks with  
505 multiple components, and hence multiple  $r$  and  $p$ -values, we calculated the weighted mean  $r$  and  
506  $p$  based on the component size. We then computed the mean  $r$  and its SD for each fragmentation  
507 step across the simulation replicates, for each one of the distance metrics and each fragmentation  
508 scenario. We only show significant correlation results ( $p < 0.05$ ) with data from 5 or more replicates.

#### 509 **4.4 Detecting early warning signals before population collapse**

510 To identify early warning signals, we computed several summary statistics of the genetic diversity  
511 ( $H_e$ ) distributions that are commonly used as early warning signals: standard deviation, skewness,  
512 and kurtosis. As the process approaches the tipping-point phase, the theoretical expectation is  
513 that the standard deviation of the  $H_e$  distribution will increase, the skewness will shift toward  
514 lower  $H_e$  values (higher asymmetry), and increased frequency of extreme values will lead to higher  
515 kurtosis [43, 45]. We did not use the lag-1 autocorrelation, although it is often used metric to  
516 measure the return rate to equilibrium after a perturbation [44], because this statistic it is designed  
517 to measure stability around a single equilibrium [44, 46], while our framework considers a series of  
518 fragmentation events between each the system arrives at migration-drift equilibrium.

519 For this analysis, we focused on autocorrelated fragmentation (Fig. 2b). We used a more  
520 connected initial network than used in previous analyses, an RGG with  $d = 0.6$ , to capture a  
521 substantial period that is far from the tipping-point phase. We ran 1000 simulations replicates and  
522 we considered two monitoring scenarios: (i) *entire metapopulation monitoring*, where we analyze  
523 the  $H_e$  distribution across all populations in the network at each step, and (ii) *single population*  
524 *monitoring*, focusing on the  $H_e$  of the final nodes to become isolated. In the latter case, we used  
525 the `generic_ews` function from the R package `earlywarnings` to apply a sliding window approach  
526 over time, with window size of 25% and default parameters without detrending or preprocessing  
527 the data.

## 528 **Data, Materials, and Software Availability**

529 All code is available in the GitHub repository at <https://github.com/Greenbaum-Lab/fragmentation.git>  
530 `tation.git`

## 531 **Acknowledgments**

532 We thank Keith Harris and Eyal Halutz for their input and assistance in the analysis. The research  
533 was funded by the Binational Science Foundation (BSF) Grant No. 2021244. OP was supported  
534 by fellowships from the Israel Ministry of Environmental Protection and from the Minerva Center  
535 for the study of Population Fragmentation (MCPF).

## 536 **Author contributions**

537 Conceptualization, OP, GG, and JK; Study design, OP, GG, and JK; Coding, OP; Analysis, OP;  
538 Writing of Original Draft, OP; Review & Editing, OP, GG, and JK; Funding Acquisition, GG and  
539 JK; Supervision, GG and JK.

## 540 **Competing interests**

541 The authors declare no competing interest.

## 542 **References**

- 543 1. Jaureguiberry, P. *et al.* The direct drivers of recent global anthropogenic biodiversity loss.  
544 *Science Advances* **8**, eabm9982 (2022).
- 545 2. Haddad, N. *et al.* Habitat fragmentation and its lasting impact on Earth’s ecosystems. *Science*  
546 *Advances* **1** (2015).
- 547 3. Van Dyck, H. & Baguette, M. Dispersal behaviour in fragmented landscapes: routine or special  
548 movements? *Basic and Applied Ecology* **6**, 535–545 (2005).
- 549 4. Fischer, J. & Lindenmayer, D. B. Landscape modification and habitat fragmentation: a syn-  
550 thesis. *Global Ecology and Biogeography* **16**, 265–280 (2007).
- 551 5. Fahrig, L. Effects of habitat fragmentation on biodiversity. *Annual Review of Ecology, Evolu-*  
552 *tion, and Systematics* **34**, 487–515 (2003).
- 553 6. Aguilar, R. *et al.* Habitat fragmentation reduces plant progeny quality: a global synthesis.  
554 *Ecology Letters* **22**, 1163–1173 (2019).
- 555 7. Reed, D. H. & Frankham, R. Correlation between fitness and genetic diversity. *Conservation*  
556 *Biology* **17**, 230–237 (2003).
- 557 8. Lowe, A., Boshier, D., Ward, M., Bacles, C. & Navarro, C. Genetic resource impacts of habitat  
558 loss and degradation; reconciling empirical evidence and predicted theory for neotropical trees.  
559 *Heredity* **95**, 255–273 (2005).
- 560 9. Charlesworth, D. & Willis, J. H. The genetics of inbreeding depression. *Nature Reviews Ge-*  
561 *netics* **10**, 783–796 (2009).
- 562 10. Jump, A. S., Marchant, R. & Peñuelas, J. Environmental change and the option value of  
563 genetic diversity. *Trends in Plant Science* **14**, 51–58 (2009).
- 564 11. Manel, S. & Holderegger, R. Ten years of landscape genetics. *Trends in Ecology & Evolution*  
565 **28**, 614–621 (2013).

- 566 12. Siol, M., Bonnin, I., Olivieri, I., Prosperi, J. & Ronfort, J. Effective population size associated  
567 with self-fertilization: lessons from temporal changes in allele frequencies in the selfing annual  
568 *Medicago truncatula*. *Journal of Evolutionary Biology* **20**, 2349–2360 (2007).
- 569 13. Kendall, K. C. *et al.* Demography and genetic structure of a recovering grizzly bear population.  
570 *The Journal of Wildlife Management* **73**, 3–16 (2009).
- 571 14. Hauser, L., Adcock, G. J., Smith, P. J., Bernal Ramírez, J. H. & Carvalho, G. R. Loss of  
572 microsatellite diversity and low effective population size in an overexploited population of  
573 New Zealand snapper (*Pagrus auratus*). *Proceedings of the National Academy of Sciences* **99**,  
574 11742–11747 (2002).
- 575 15. Wright, S. *The roles of mutation, inbreeding, crossbreeding and selection in evolution* in *Pro-*  
576 *ceedings of the Sixth International Congress of Genetics* **1** (1932), 356–366.
- 577 16. Levene, H. Genetic equilibrium when more than one ecological niche is available. *The American*  
578 *Naturalist* **87**, 331–333 (1953).
- 579 17. Kimura, M. & Weiss, G. H. The stepping stone model of population structure and the decrease  
580 of genetic correlation with distance. *Genetics* **49**, 561 (1964).
- 581 18. Wright, S. Isolation by distance. *Genetics* **28**, 114 (1943).
- 582 19. Wright, S. Evolution in Mendelian populations. *Genetics* **16**, 97 (1931).
- 583 20. Sexton, J. P., Hangartner, S. B. & Hoffmann, A. A. Genetic isolation by environment or  
584 distance: which pattern of gene flow is most common? *Evolution* **68**, 1–15 (2014).
- 585 21. Harris, L. D. & Silva-Lopez, G. *Forest fragmentation and the conservation of biological diver-*  
586 *sity* in *Conservation biology: The theory and practice of nature conservation preservation and*  
587 *management* (Springer, 1992), 197–237.
- 588 22. Greenbaum, G. & Fefferman, N. H. Application of network methods for understanding evolu-  
589 tionary dynamics in discrete habitats. *Molecular Ecology* **26**, 2850–2863 (2017).
- 590 23. Dyer, R. J. & Nason, J. D. Population graphs: the graph theoretic shape of genetic structure.  
591 *Molecular Ecology* **13**, 1713–1727 (2004).
- 592 24. Rozenfeld, A. F. *et al.* Network analysis identifies weak and strong links in a metapopulation  
593 system. *Proceedings of the National Academy of Sciences* **105**, 18824–18829 (2008).
- 594 25. Dyer, R. J., Nason, J. D. & Garrick, R. C. Landscape modelling of gene flow: improved power  
595 using conditional genetic distance derived from the topology of population networks. *Molecular*  
596 *Ecology* **19**, 3746–3759 (2010).
- 597 26. Ball, M. C., Finnegan, L., Manseau, M. & Wilson, P. Integrating multiple analytical ap-  
598 proaches to spatially delineate and characterize genetic population structure: an application  
599 to boreal caribou (*Rangifer tarandus caribou*) in central Canada. *Conservation Genetics* **11**,  
600 2131–2143 (2010).

- 601 27. Munwes, I. *et al.* The change in genetic diversity down the core-edge gradient in the eastern  
602 spadefoot toad (*Pelobates syriacus*). *Molecular Ecology* **19**, 2675–2689 (2010).
- 603 28. Fitzpatrick, J., Carlon, D., Lippe, C. & Robertson, D. R. The West Pacific diversity hotspot as  
604 a source or sink for new species? Population genetic insights from the Indo-Pacific parrotfish  
605 *Scarus rubroviolaceus*. *Molecular Ecology* **20**, 219–234 (2011).
- 606 29. Garroway, C. J., Bowman, J. & Wilson, P. J. Using a genetic network to parameterize a  
607 landscape resistance surface for fishers, *Martes pennanti*. *Molecular Ecology* **20**, 3978–3988  
608 (2011).
- 609 30. Paschou, P. *et al.* Maritime route of colonization of Europe. *Proceedings of the National*  
610 *Academy of Sciences* **111**, 9211–9216 (2014).
- 611 31. Werth, S. & Scheidegger, C. Gene flow within and between catchments in the threatened  
612 riparian plant *Myricaria germanica*. *PLOS One* **9**, e99400 (2014).
- 613 32. Windmaißer, T., Kattari, S., Heubl, G. & Reisch, C. Glacial refugia and postglacial expansion  
614 of the alpine–prealpine plant species *Polygala chamaebuxus*. *Ecology and Evolution* **6**, 7809–  
615 7819 (2016).
- 616 33. Fahrig, L. Ecological responses to habitat fragmentation per se. *Annual Review of Ecology,*  
617 *Evolution, and Systematics* **48**, 1–23 (2017).
- 618 34. Alcala, N., Goldberg, A., Ramakrishnan, U. & Rosenberg, N. A. Coalescent theory of migration  
619 network motifs. *Molecular Biology and Evolution* **36**, 2358–2374 (2019).
- 620 35. Wilkinson-Herbots, H. M. Genealogy and subpopulation differentiation under various models  
621 of population structure. *Journal of Mathematical Biology* **37**, 535–585 (1998).
- 622 36. Slatkin, M. Inbreeding coefficients and coalescence times. *Genetics Research* **58**, 167–175  
623 (1991).
- 624 37. Dall, J. & Christensen, M. Random geometric graphs. *Physical Review E* **66**, 016121 (2002).
- 625 38. Kimura, M. Theoretical foundation of population genetics at the molecular level. *Theoretical*  
626 *Population Biology* **2**, 174–208 (1971).
- 627 39. Rodrigues, F. A. *Network centrality: an introduction in A mathematical modeling approach*  
628 *from nonlinear dynamics to complex systems* (Springer, 2018), 177–196.
- 629 40. Rodger, Y. S., Greenbaum, G., Silver, M., Bar-David, S. & Winters, G. Detecting hierarchical  
630 levels of connectivity in a population of *Acacia tortilis* at the northern edge of the species’  
631 global distribution: Combining classical population genetics and network analyses. *PLOS One*  
632 **13**, e0194901 (2018).
- 633 41. Malécot, G. *Quelques schémas probabilistes sur la variabilité des populations naturelles in*  
634 *Annales de l’Université de Lyon A* **13** (1950), 37–60.
- 635 42. Scheffer, M., Carpenter, S., Foley, J. A., Folke, C. & Walker, B. Catastrophic shifts in ecosys-  
636 tems. *Nature* **413**, 591–596 (2001).

- 637 43. Scheffer, M. *et al.* Early-warning signals for critical transitions. *Nature* **461**, 53–59 (2009).
- 638 44. Dakos, V. *et al.* Methods for detecting early warnings of critical transitions in time series  
639 illustrated using simulated ecological data. *PLOS One* **7**, e41010 (2012).
- 640 45. Guttal, V. & Jayaprakash, C. Changing skewness: an early warning signal of regime shifts in  
641 ecosystems. *Ecology Letters* **11**, 450–460 (2008).
- 642 46. Veraart, A. J. *et al.* Recovery rates reflect distance to a tipping point in a living system.  
643 *Nature* **481**, 357–359 (2012).
- 644 47. Hanski, I. Habitat fragmentation and species richness. *Journal of Biogeography* **42** (2015).
- 645 48. Watson, D. *et al.* Monitoring ecological consequences of efforts to restore landscape-scale  
646 connectivity. *Biological Conservation* **206**, 201–209 (2017).
- 647 49. Frankham, R. Challenges and opportunities of genetic approaches to biological conservation.  
648 *Biological Conservation* **143**, 1919–1927 (2010).
- 649 50. Schwartz, M. K., Luikart, G. & Waples, R. S. Genetic monitoring as a promising tool for  
650 conservation and management. *Trends in Ecology & Evolution* **22**, 25–33 (2007).
- 651 51. Riitters, K., Wickham, J., O’Neill, R., Jones, B. & Smith, E. Global-scale patterns of forest  
652 fragmentation. *Conservation Ecology* **4** (2000).
- 653 52. Keyghobadi, N., Roland, J., Matter, S. & Strobeck, C. Among- and within-patch compo-  
654 nents of genetic diversity respond at different rates to habitat fragmentation: an empirical  
655 demonstration. *Proceedings of the Royal Society B: Biological Sciences* **272**, 553–560 (2005).
- 656 53. Allendorf, F. W. Genetic drift and the loss of alleles versus heterozygosity. *Zoo Biology* **5**,  
657 181–190 (1986).
- 658 54. Templeton, A. R. *Population genetics and microevolutionary theory* (John Wiley & Sons,  
659 2021).
- 660 55. Templeton, A. R. Mechanisms of speciation—a population genetic approach. *Annual Review*  
661 *of Ecology and Systematics*, 23–48 (1981).
- 662 56. Andren, H. Effects of habitat fragmentation on birds and mammals in landscapes with different  
663 proportions of suitable habitat: a review. *Oikos*, 355–366 (1994).
- 664 57. Andren, H. Population responses to habitat fragmentation: statistical power and the random  
665 sample hypothesis. *Oikos*, 235–242 (1996).
- 666 58. Pardini, R., Bueno, A., Gardner, T., Prado, P. & Metzger, J. Beyond the fragmentation  
667 threshold hypothesis: Regime shifts in biodiversity across fragmented landscapes. *PLOS One*  
668 **5** (2010).
- 669 59. Hoffmann, A. A. & Willi, Y. Detecting genetic responses to environmental change. *Nature*  
670 *Reviews Genetics* **9**, 421–432 (2008).

- 671 60. Dakos, V. *et al.* Slowing down as an early warning signal for abrupt climate change. *Proceedings*  
672 *of the National Academy of Sciences* **105**, 14308–14312 (2008).
- 673 61. Epperson, B. K. *Geographical genetics (MPB-38)* (Princeton University Press, 2003).
- 674 62. Crispo, E. & Hendry, A. Does time since colonization influence isolation by distance? A meta-  
675 analysis. *Conservation Genetics* **6**, 665–682 (2005).
- 676 63. Jenkins, D. G. *et al.* A meta-analysis of isolation by distance: relic or reference standard for  
677 landscape genetics? *Ecography* **33**, 315–320 (2010).
- 678 64. Storfer, A., Murphy, M. A., Spear, S. F., Holderegger, R. & Waits, L. P. Landscape genetics:  
679 where are we now? *Molecular Ecology* **19**, 3496–3514 (2010).
- 680 65. Ramachandran, S. *et al.* Support from the relationship of genetic and geographic distance in  
681 human populations for a serial founder effect originating in Africa. *Proceedings of the National*  
682 *Academy of Sciences* **102**, 15942–15947 (2005).
- 683 66. Gómez-Fernández, A., Alcocer, I. & Matesanz, S. Does higher connectivity lead to higher ge-  
684 netic diversity? Effects of habitat fragmentation on genetic variation and population structure  
685 in a gypsophile. *Conservation Genetics* **17**, 631–641 (2016).
- 686 67. Wasserman, T. N., Cushman, S. A., Littell, J. S., Shirk, A. J. & Landguth, E. L. Population  
687 connectivity and genetic diversity of American marten (*Martes americana*) in the United  
688 States northern Rocky Mountains in a climate change context. *Conservation Genetics* **14**,  
689 529–541 (2013).
- 690 68. Jangjoo, M., Matter, S. F., Roland, J. & Keyghobadi, N. Connectivity rescues genetic diversity  
691 after a demographic bottleneck in a butterfly population network. *Proceedings of the National*  
692 *Academy of Sciences* **113**, 10914–10919 (2016).
- 693 69. Kool, J. T., Moilanen, A. & Treml, E. A. Population connectivity: recent advances and new  
694 perspectives. *Landscape Ecology* **28**, 165–185 (2013).
- 695 70. Crow, J. F. & Aoki, K. Group selection for a polygenic behavioral trait: estimating the degree  
696 of population subdivision. *Proceedings of the National Academy of Sciences* **81**, 6073–6077  
697 (1984).
- 698 71. Varvio, S.-L., Chakraborty, R. & Nei, M. Genetic variation in subdivided populations and  
699 conservation genetics. *Heredity* **57**, 189–198 (1986).
- 700 72. Barthélemy, M. Spatial networks. *Physics Reports* **499**, 1–101 (2011).
- 701 73. Penrose, M. *Random geometric graphs* (OUP Oxford, 2003).
- 702 74. Marsh, L. K. *The nature of fragmentation in Primates in fragments: Ecology and conservation*  
703 (Springer, 2003), 1–10.
- 704 75. Erdős, P., Rényi, A., *et al.* On the evolution of random graphs. *Publications of the Mathemat-*  
705 *ical Institute of the Hungarian Academy of Sciences* **5**, 17–60 (1960).

- 706 76. Sen, P., Banerjee, K. & Biswas, T. Phase transitions in a network with a range-dependent  
707 connection probability. *Physical Review E* **66**, 037102 (2002).
- 708 77. Newman, M. E. & Watts, D. J. Scaling and percolation in the small-world network model.  
709 *Physical Review E* **60**, 7332 (1999).
- 710 78. Eppstein, D. Finding the  $k$  shortest paths. *SIAM Journal on Computing* **28**, 652–673 (1998).
- 711 79. Noh, J. D. & Rieger, H. Random walks on complex networks. *Physical Review Letters* **92**,  
712 118701 (2004).